Applied Catalysis B: Environmental 163 (2015) 520–530

Contents lists available at ScienceDirect

Applied Catalysis B: Environmental

journal homepage: www.elsevier.com/locate/apcatb

Conversion of 5-hydroxymethylfurfural to 2,5-furandicarboxylic acid over Au-based catalysts: Optimization of active phase and metal–support interaction

Stefania Albonetti[a,c,*], Alice Lolli[a,c], Vittorio Morandi[b], Andrea Migliori[b], Carlo Lucarelli[d,c], Fabrizio Cavani[a,c]

[a] Dip. Chimica Industriale "Toso Montanari", Viale Risorgimento 4, 40136 Bologna, Italy
[b] CNR-IMM Section of Bologna, Via Gobetti 101, 40129 Bologna, Italy
[c] Consorzio INSTM–UdR Bologna, Via G. Giusti, 9, 50121 Florence, Italy
[d] Dipartimento di Scienza e Alta Tecnologia, University of Insubria, Via Valleggio 11, 22100 Como, Italy

ARTICLE INFO

Article history:
Received 5 June 2014
Received in revised form 5 August 2014
Accepted 19 August 2014
Available online 23 August 2014

Keywords:
HMF
2,5-Furandicarboxylic acid
Gold–copper catalysts
CeO_2

ABSTRACT

In the present work, a series of Au- and Au–Cu-containing catalysts based on different carriers such as TiO_2 and CeO_2 were studied with a view to increasing the activity and selectivity in 5-hydroxymethylfurfural oxidation by optimizing the interaction both between the metals and with the support. The results obtained demonstrated the high activity in HMF oxidation of gold supported on ceria and titania. Nevertheless, although the particle size of gold on both supports was comparable, Au/CeO_2 showed significantly higher activity than Au/TiO_2, thus corroborating the theory that not only the gold particle size, but the support also, plays a key role in HMF oxidation in the aqueous phase. Indeed, pre-made uniform nanoparticles, used for catalyst preparation, were surface-bound by poly(N-vinyl-2-pyrrolidone) – the stabilizer used during nanoparticle synthesis – whose presence proved to prevent the interaction of active phases with CeO_2, while worsening the catalytic activity of both monometallic and bimetallic systems. The pre-treatment of the prepared catalysts was necessary to activate the materials, by maximizing the contact between the metal and the support and thus suggesting an important role of the ceria defects on 5-hydroxymethylfurfural oxidation to 2,5-furandicarboxylic acid.

1. Introduction

In the 21st century, the main issues concerning the use of fossil fuels for the production of energy and chemicals are their limited availability (being non-renewable) and the pollution caused by their use. The greenhouse effect, increased by the massive use of these non-renewable resources, is one of the world's major problems today. Biomasses are currently the most promising alternative to fossil hydrocarbons for the production of chemicals and fuels [1,2]. Nevertheless, the use of biomasses has sparked several controversies concerning ethical issues, for example the production of bio-ethanol, which uses mainly corn and sugar cane as raw materials [3]. For these reasons, today research is moving toward the use of biomasses derived from non-cultivable land and inedible raw materials, such as ligno-cellulosics [4,5].

In the transformation of biomasses into chemicals, an important role is played by furfural derivatives which have functional groups in position five [6,7]. For instance, 5-hydroxymethyl-2-furfural (HMF) is a key precursor for the synthesis of derivatives with applications in the pharmaceutical and polymer industry [8–11]; it can be oxidized to obtain 2,5-furandicarboxylic acid (FDCA), a monomer for the synthesis of a new class of polymers, alternative to those obtained from terephthalic acid. The Department of Energy identifies FDCA as a key platform molecule serving as a starting point for the synthesis of various polymers. The preparation of FDCA from HMF has been studied widely over the past 20 years and various methods have been proposed for this oxidative process. Studied paths range from the use of stoichiometric oxidants to heterogeneous metal catalysts or biochemical production [12,13]. At the present time, there is no commercial process available for producing FDCA. However Avantium, among others, is pursuing the use of FDCA to produce polyethylene furandicarboxylate (PEF) by replacing terephthalic acid, as shown in Scheme 1.

The exact route followed for HMF oxidation has not yet been disclosed, but the current technology for terephthalic acid production

* Corresponding author. Tel.: +39 0512093681; fax: +39 0512093679.
E-mail address: stefania.albonetti@unibo.it (S. Albonetti).

http://dx.doi.org/10.1016/j.apcatb.2014.08.026
0926-3373/

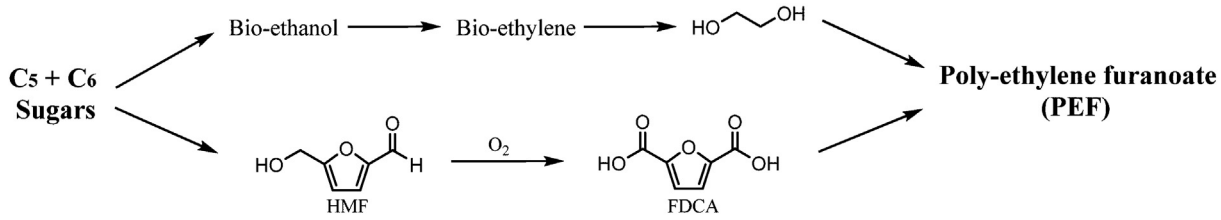

Scheme 1. The process for PFE production from monosaccharides.

using cobalt–manganese–bromide catalyst is likely being evaluated. This system has some drawbacks in its use of corrosive media and dangerous compounds, which make it an environmentally unfriendly process [14–16]. Moreover, there are concerns regarding the purity of both the product and the final polymer.

Recently, Au-supported catalysts have been found to be very active for HMF oxidation to FDCA [17,18]. Many researchers have focused their attention on the study of the best supports and reaction conditions for improving FDCA yield [19–21]. Nevertheless, catalyst stability and process productivity remain low. According to the current research status, the preparation of bimetallic catalysts with controlled size and composition over different supports may be a promising way to improve catalyst activity and stability [23,24]. Traditional synthetic techniques for supported metal catalysts typically involve the deposition of metal precursors onto high surface area supports, followed by various thermal activation treatments. Nevertheless, with bimetallic systems these methods often provide limited control over the structure and composition of bimetallic species, thus leading to significant non-uniformity in composition from particle to particle. The preparation of preformed colloidal nano-sols has been used for the controlled synthesis of monometallic and bimetallic catalysts [25,26] with steric stabilizers such as polyvinylpyrrolidone (PVP) to protect nanoparticles from excessive growth [27,28]. Numerous examples of such catalytic systems have been documented in literature for oxidation reactions [29,30].

Nanoparticle homogeneity is of crucial importance in relating the catalytic activity with the nature of active species and the role of its interaction with the support. This factor is even more significant when it comes to the comparison of bimetallic and monometallic nanoparticles. Thus the colloidal nanoparticle size and structure control techniques become particularly advantageous in elucidating mechanisms over bimetallic catalysts.

In our previous works [23,31] we synthesized titania-supported Au and Au/Cu species by using PVP-stabilized sols with controlled size, structure, and composition prepared using an original process in water [32]. Unprecedented catalytic activity and stability were obtained with these catalytic materials in the oxidation of HMF to FDCA. Well-defined Au–Cu alloy nanoparticles supported on anatase TiO_2 were considerably more active and selective toward HMF oxidation than their monometallic counterparts (i.e. Au/TiO_2 and Cu/TiO_2): this may be ascribed to Au site isolation effects caused by alloying. Moreover, reusability tests show that the Au–Cu-based catalysts were significantly more stable than gold ones [23].

In the present study, we investigated the preparation, characterization, and catalytic activity of CeO_2-supported Au, Cu and Au–Cu nanoparticles synthesized as metal colloids. We also compared the established properties with those of analogous TiO_2-supported materials in order to optimize the catalyst activity in the selective oxidation of HMF over these Au-based catalysts by tuning active-phase composition and metal–support interaction. Among different bimetallic catalysts, Au–Cu materials have recently attracted interest for the catalytic oxidation of CO, benzyl alcohol and propene [33–35] as well as for the partial oxidation of methanol and ethanol [36,37]. No systematic studies reporting the use of colloidal Cu and Au nanoparticles in the preparation of heterogeneous catalysts are available, however, in open literature. Therefore, further insight into the role of active phase/metal oxide interface in HMF oxidation reaction may be gained by using size-controlled Au and Au–Cu nanoparticles whose particle size is established before the deposition on the metal oxide support. Indeed, in this case the effect of oxide supports in determining the size and dispersion of the active phase is minimized because nanoparticles were synthesized before being immobilized on the oxide surface. Moreover, since the preparation of metal sols typically requires the use of polymer ligands to control metal nanoparticle growth and to stabilize colloids [38,39], the effects of possible residual polymers attached to the metal surface and to the support during the immobilization process were investigated and discussed.

2. Experimental

2.1. Catalyst preparation

Au/CeO_2, Au/TiO_2, and bimetallic Au–Cu supported catalysts were prepared by the immobilization of preformed monometallic and bimetallic colloids on CeO_2 (VP AdNano 90, Evonik) and TiO_2 (DT51 Millennium Chemicals) surfaces. Mono and bimetallic nanoparticles were prepared using the method previously developed [23]. In brief, the necessary quantity of poly(vinylpyrrolidone) (PVP K25, Sigma Aldrich, MW ≈ 29,000) used as a nanoparticle stabilizer was added to a solution of NaOH in water. The solution was then heated to 95 °C. At this temperature, β-D-glucose (Fluka) and an aqueous solution containing the metal precursors ($HAuCl_4$ and $CuSO_4{\cdot}5H_2O$) in the desired ratio were added and stirred for 2.5 min. The ratio among PVP, β-D-glucose, NaOH, and metals was optimized for each gold and copper content [40–42]. Glucose and PVP metal ratios were selected to obtain small particle sizes with both monometallic and bimetallic sols, thus requiring a significantly higher quantity of PVP and glucose for bimetallic systems to foster particle nucleation instead of particle growth. In particular, Au, Au_3Cu_1, Au_1Cu_1, and Au_1Cu_3 sols were prepared by using PVP monomer/total metals molar ratios equal to 2.8, 5.8, 8.9, and 12, respectively. Before use, the as-prepared sols were concentrated and washed with distilled water using 50 kDa Amicon Ultra filters (Millipore) to eliminate the excess PVP and other reagents dissolved in the aqueous media. Then Au and Au–Cu colloids were impregnated onto both TiO_2 and CeO_2 supports by maintaining the total metal loading at 1.5 wt%, while the Au:Cu ratio varied from 1:0 to 1:3 on a molar basis. For all the samples, the impregnation solvent was evaporated by thermal treatment at 120 °C. Some samples were calcined at 300 °C. Catalyst samples are denoted as Au–S and Au_xCu_y–S, where *x* and *y* refer to the Au:Cu molar ratio and S to the support (i.e. Au_1Cu_1–Ce indicates a CeO_2-supported sample synthesized with 1.5 wt% of bimetallic nanoparticles with an Au:Cu molar ratio of 1). Catalysts were characterized in detail by XRD, HR-TEM TGA, and BET analysis. To compare catalysts with a reference, monometallic Au–Ce material was prepared by the deposition/precipitation method (see data reported in Figure S1).

Table 1
Structural parameters and chemical composition of Au and Au–Cu supported on CeO_2 and TiO_2.

Catalyst	Total metal loading (wt%)	Au content (wt%)	Cu content (wt%)	Surface area (m^2/g)	Au crystallite size (nm)[a]
CeO_2	–	–	–	89	–
Au–Ce	1.5	1.5	–	85	6.0
Au_3Cu_1–Ce	1.5	1.34	0.16	62	5.0
Au_1Cu_1–Ce	1.5	1.14	0.36	53	5.0
Au_1Cu_3–Ce	1.5	0.76	0.74	49	5.0
TiO_2	–	–	–	83	–
Au–Ti	1.5	1.5	-	74	6.5
Au_3Cu_1–Ti	1.5	1.34	0.16	72	5.0
Au_1Cu_1–Ti	1.5	1.14	0.36	64	5.0
Au_1Cu_3–Ti	1.5	0.76	0.74	60	5.0

[a] Estimated from XRD.

However, this method cannot be applied for the preparation of bimetallic systems. Table 1 shows the composition and characteristics of the catalysts studied in this work.

2.2. Analytical methods

Catalyst surface areas were measured by N_2 physisorption apparatus (Sorpty 1750 CE instruments) and the single-point BET analysis method, in which samples were pre-treated under vacuum conditions at 120 °C.

XRD measurements were carried out at room temperature with a Bragg/Brentano diffractometer (X'pertPro PANalytical) equipped with a fast X'Celerator detector, using a Cu anode as the X-ray source (Kα, λ = 1.5418 Å). All catalysts were analyzed in the region of 10–80° 2θ, counting for 20 s at each 0.05° step. However, for the evaluation of the metal crystallite size for the supported catalysts, a second acquisition was performed in the 2θ range 36–46°, counting for 400 s at each 0.03 step. In fact, the coherence length of the Au crystalline domains was evaluated through the single-line profile fitting of the reflection at 2θ 38.2° for Au–CeO_2 catalysts. Crystallite size values were calculated using the Scherrer equation from the full width at half maximum intensity measurements.

Transmission Electron Microscopy (TEM) observations were made using a FEI Tecnai F20 TEM equipped with a Schottky emitter and operating at 200 keV. The instrument is equipped with a Fischione High Angle Annular Dark Field Detector (HAADF) for Scanning Transmission Electron Microscopy (STEM) investigations and with an Energy Dispersive X-Ray Spectrometer (EDX) for X-ray microanalysis. Samples were ground in a mortar and treated with ultrasounds in isopropyl alcohol. A droplet of the resulting finely dispersed suspension was evaporated at room temperature and under atmospheric pressure on a holey carbon film.

To verify the behavior of different samples under thermogravimetric analysis, TGA was obtained using a Rheometric Scientific STA1500 analyzer while heating the sample in air from 25 °C to 600 °C.

The oxidation behavior of different samples was studied via Temperature Programmed Oxidation using a Thermoquest TPDRO instrument under 5% O_2/He flow (20 mL min^{-1}). The temperature was raised from 60 to 650 °C with a heating rate of 10 °C min^{-1} followed by an isothermal step at 650 °C for 30 min.

2.3. Oxidation of HMF

The oxidation of HMF was carried out using an autoclave reactor of 100 mL capacity, equipped with a mechanical stirrer (0–600 rpm) and measurement tools for temperature and pressure. The reactor was charged with an aqueous solution (25 mL distilled water) containing the appropriate amount of HMF, base (NaOH) and catalyst (HMF/metal molar ratio = 100). The autoclave was purged 3 times with O_2 (5 bar) and then pressurized at 10 bar. If not indicated otherwise, the temperature was increased to 70 °C and the reaction mixture was stirred at approximately 400 rpm for 4 h. Initial time (time zero) for the reaction was taken when the set point temperature was reached (after 15 min of heating). At the end of the reaction, the reactor was cooled down to room temperature and the solution was filtered. Then, 4 mL of water were added to an aliquot of the reaction solution (1 mL) before analysis with an Agilent Infinity 1260 liquid chromatograph equipped with a Aminex HPX-87H 300 mm × 7.8 mm column using a 0.005 M H_2SO_4 solution as mobile phase. The compound identification was achieved by calibration using reference commercial samples.

3. Results and discussion

3.1. Catalysts characterization

The surface area and average Au crystal size for the prepared catalysts are listed in Table 1. Surface areas similar to supports were obtained in the case of gold supported on TiO_2 and CeO_2, thus indicating that gold nanoparticle deposition did not lead to a significant change in the texture of supporting materials. Conversely, the impregnation with bimetallic Au–Cu sols indicated that the deposition somewhat affects the textural properties of ceria and titania, while samples with the lowest Au:Cu metal ratio showed a significant reduction in the surface area. This is probably due to the presence of a higher organic content in bimetallic systems. As a matter of fact, the organic layer surrounding metal nanoparticles may occlude the oxide porosity, thus leading to a decrease in the surface area. To confirm this hypothesis, the as-synthesized materials were characterized by TGA and DTA (Fig. 1A and B). The TGA curves of the as-synthesized ceria-supported samples (Fig. 1A) show two distinct weight losses; (i) a lower weight loss between 50 and 150 °C, due to the physically adsorbed water, and (ii) a higher weight loss, in the temperature range of 200–300 °C, which is associated with an exothermal process (Fig. 1B) ascribable to the burning-off of the adsorbed poly(N-vinyl-2-pyrrolidone) (PVP) in the sample. Indeed, the decomposition of PVP has been reported to occur at higher temperatures (400–600 °C) in the absence of active metals [43,44], but between 200 °C and 450 °C in the presence of noble metals such as Pt [45]. The observed catalyst's weight loss in TG analysis increased from approximately 2 wt% to 10 wt% by increasing the Cu content in the materials (Table 2).

During sol preparation, the weight ratios of PVP to total metals varied from 2.8 to 12, while the metal loading was always equal to 1.5 wt%; therefore, the observed increase in the weight loss may be attributed mainly to the highest amount of PVP present over samples with the highest Cu content. These results are confirmed by the comparison of the weight loss observed for TiO_2-supported materials (Table 2) prepared using the same preformed sols [29], which show exactly the same trend. In addition, the exothermicity associated with the PVP decomposition significantly increased by

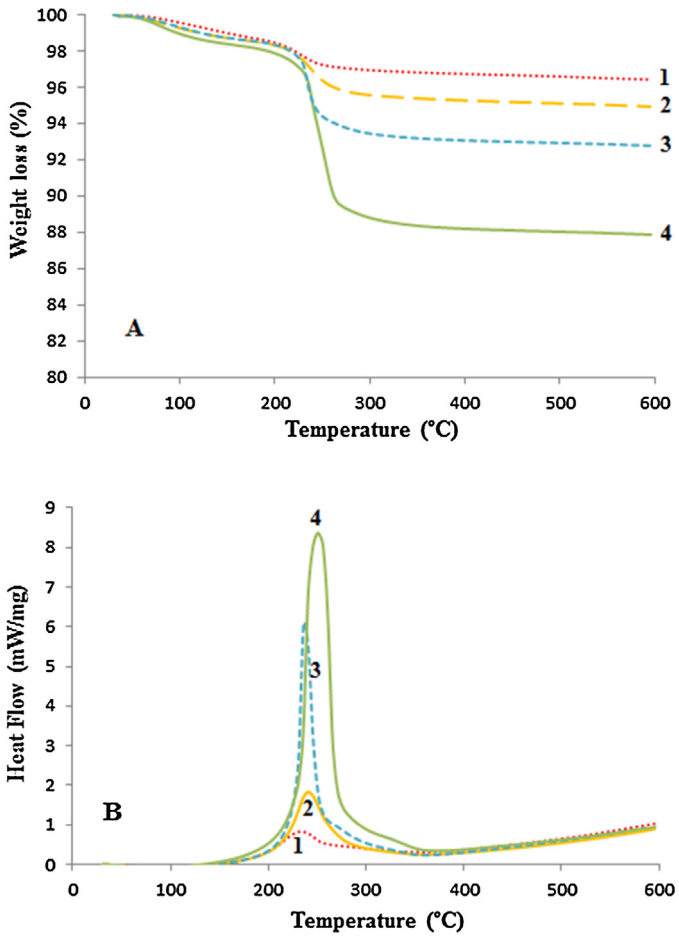

Fig. 1. Thermogravimetric analysis (A) and differential thermal analysis (B) in air of CeO_2-supported catalysts with different Au:Cu atomic ratios. (1) Au–Ce; (2) Au_3Cu_1–Ce; (3) Au_1Cu_1–Ce; (4) Au_1Cu_3–Ce.

Table 2
Weight loss and PVP decomposition temperature of the Au and Au–Cu supported on CeO_2 and TiO_2.

Catalyst	T (°C)	Weight loss (%)
Au–Ce	236	1.9
Au_3Cu_1–Ce	240	3.1
Au_1Cu_1–Ce	236	5.4
Au_1Cu_3–Ce	250	9.7
Au–Ti	312	2.0
Au_3Cu_1–Ti	310	3.5
Au_1Cu_1–Ti	320	5.5
Au_1Cu_3–Ti	301	9.8

increasing the Cu content in the active phase (Fig. 1B); this trend explains the decrease observed in the surface area of the catalysts with high Cu content. Moreover, the data in this table show that the temperature of PVP combustion depends on the support, thus indicating that ceria promotes PVP decomposition.

Fig. 2 shows XRD patterns for Au and Au–Cu catalysts at different metal ratios. This analysis revealed the presence of diffraction peaks related to the CeO_2 phase in the cubic crystal structure of fluorite-type, while no peaks related to Au species were evidenced using standard XRD acquisition procedures, thus suggesting that very small Au and Au–Cu nanoparticles were formed: a fact which is consistent with the previous findings [31]. However, when a more accurate XRD acquisition was used, a small broad peak at about 38.2° 2θ was evidenced, which was attributed to metallic Au and/or the Au–Cu alloy. The average diameters of the metallic particles, estimated from this peak by Scherrer's equation, are given in Table 1. Very small Au particles were obtained in all samples.

Au and Au–Cu species over CeO_2 were investigated using high-resolution TEM imaging. Fig. 3A and B shows some representative TEM images of the Au and Au–Cu supported catalysts and the corresponding size distribution histograms. Dispersed agglomerates include ceria particles with a mean diameter of 10–15 nm. Au and Au–Cu nanoparticles are embedded in the ceria network. This study reveals a significant homogeneity in the size distribution of Au and Au–Cu particles supported on TiO_2 and CeO_2. Both metals are in close contact with the supports, and dark field images (not shown) confirm that the metallic nanoparticles are evenly distributed. Au

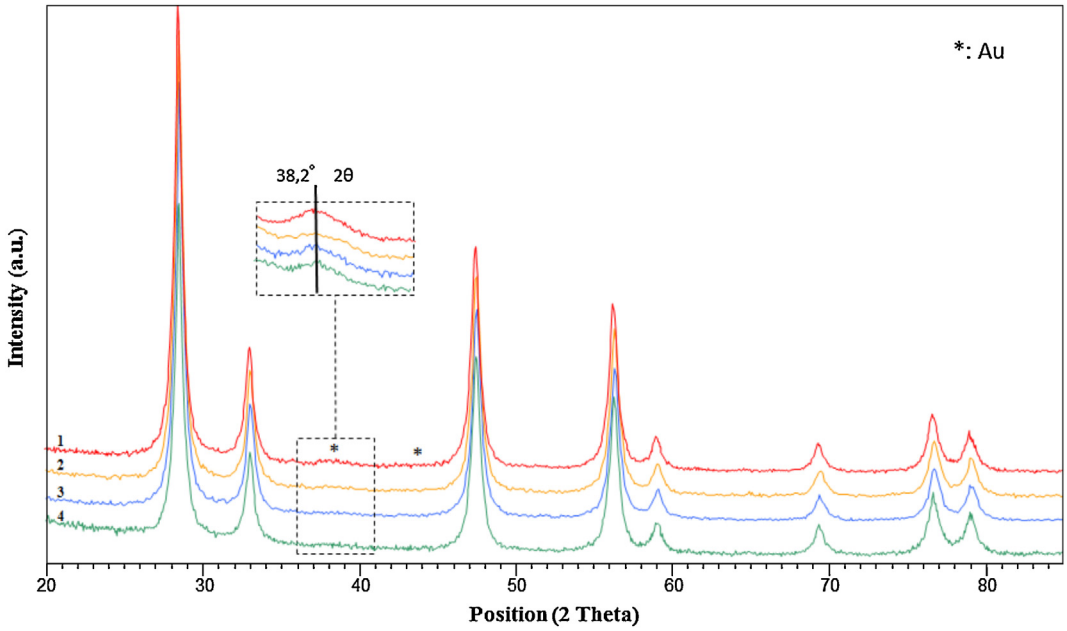

Fig. 2. XRD patterns of CeO_2-supported catalysts with different Au:Cu atomic ratios. (1) Au–Ce; (2) Au_3Cu_1–Ce; (3) Au_1Cu_1–Ce; (4) Au_1Cu_3–Ce. Inset: magnification of the reflection at 2θ 38,2° which was used to evaluate the Au crystal size.

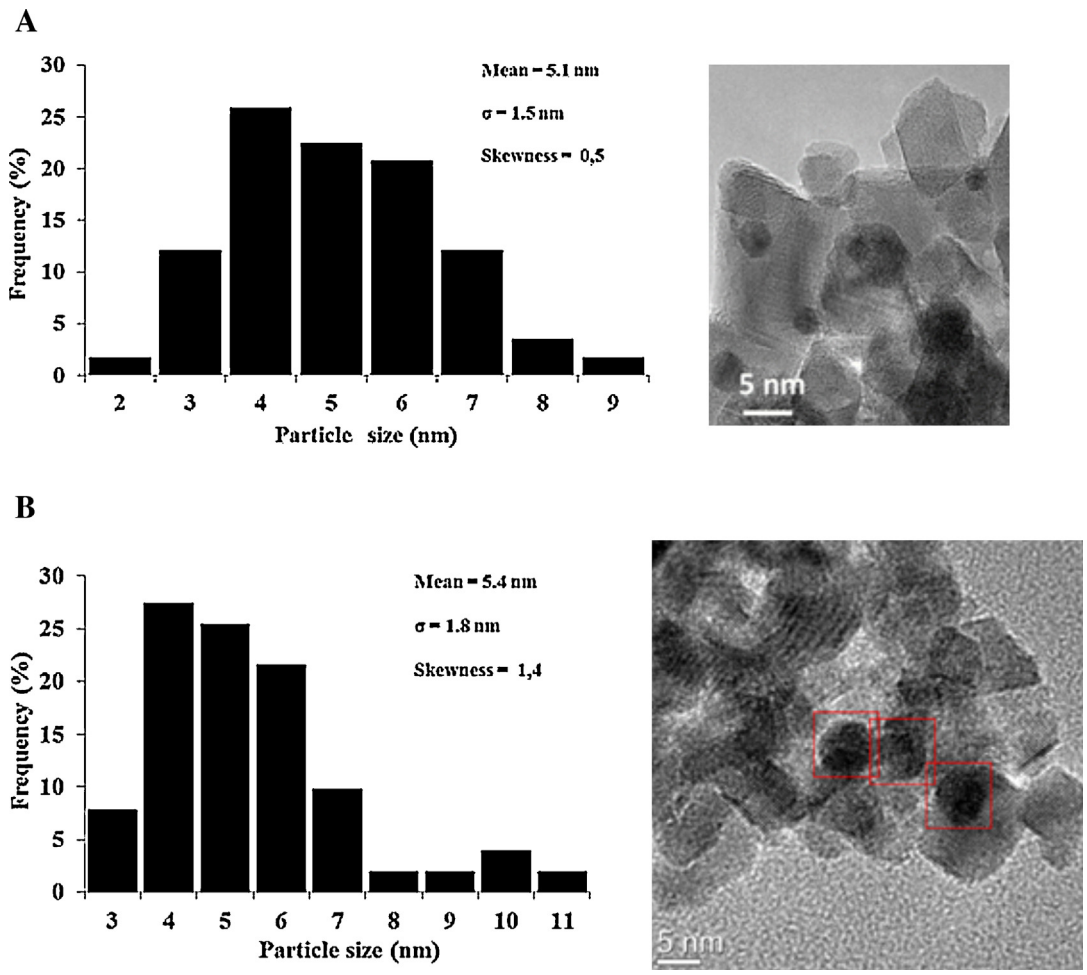

Fig. 3. Representative TEM images of the Au- and Au–Cu-supported catalysts. (A) Au–Ce sample dried at 120 °C and (B) Au_3Cu_1–Ce sample dried at 120 °C.

and Au–Cu nanoparticles are present in an almost spherical shape with very narrow diameter distribution (5–6 nm), thus confirming the results obtained from XRD.

3.2. Catalytic tests

3.2.1. HMF conversion in blank experiments

Preliminary experiments have been devoted to blank tests, by reacting HMF in an aqueous solution with HMF:NaOH ratio of 1:4, at 70 °C and ambient pressure, both under air and under N_2, in the absence of any catalytic system (Fig. 4). These experiments made it possible to verify that no oxidation occurred under these conditions; however, as already reported in our previous work [23] and in the recent Vuyyuru paper [46], a significant amount of HMF was degraded in these basic conditions. Fig. 4 shows 40% of HMF conversion at 70 °C already after 10 min, without the formation of any detectable oxidation products. The reaction mixture turned from colorless to yellow and then to red with the reaction time. After 30 min, HMF was totally converted and the solution became brownish. The formed degradation products were soluble in water at high pH (pH = 13), but they were insoluble in acidic conditions. In fact, when some drops of HCl were added, the formation of a black precipitate was observed. In these reaction conditions, aldol condensation should not be possible due to the absence of species with alpha H atoms; therefore, the mechanism should be different from that obtained in acidic conditions [47]. However, even if these degradation products are formed with a different reaction

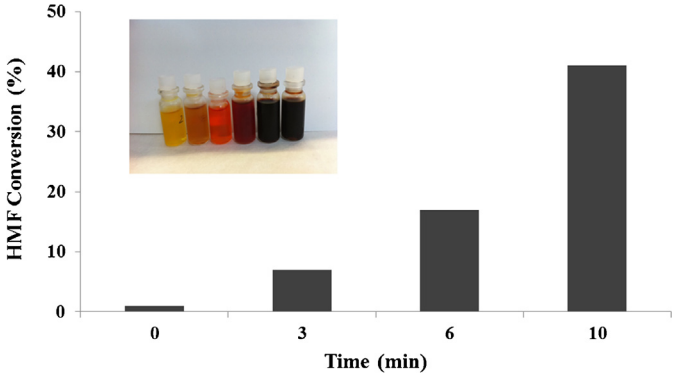

Fig. 4. Effect of reaction time on HMF degradation. Reaction conditions: no catalyst, no O_2 pressure, temperature 70 °C, ambient pressure, HMF:NaOH 1:4 molar ratio.

pathway, they behave like humins, which are formed in acidic conditions. Indeed, Piccolo et al. [48] have treated some organic matter in basic conditions by using NaOH and obtained the precipitation of some humic acids by lowering the pH with HCl to the value of 1.

Generally speaking, humins have coiled conformations which are cross-linked by weak forces such as Van der Waals bonds, but when the pH is lowered, both the formation of intermolecular hydrogen bonds and the rearrangement of the conformation are observed. It is probable that the HMF degradation products, obtained in basic conditions, are similar to humins and are arranged

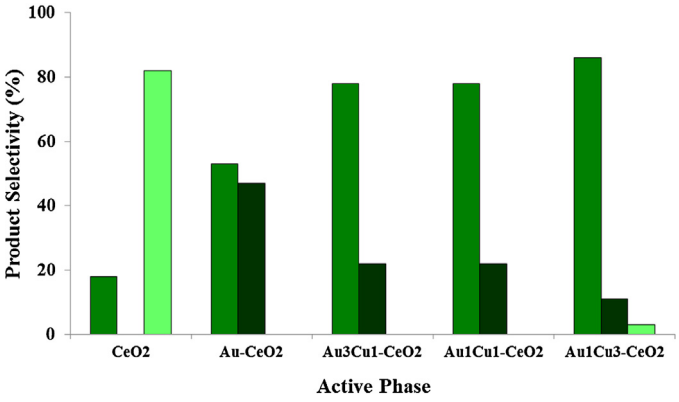

Fig. 5. Product selectivity on CeO_2-supported catalysts at different Au:Cu atomic ratios. Results are given at total conversion of HMF. Reaction conditions: temperature 70 °C, reaction time 240 min, O_2 pressure 10 bar, HMF:metal:NaOH molar ratio 1:0.01:4. Legend: HMFCA, FDCA, by-products.

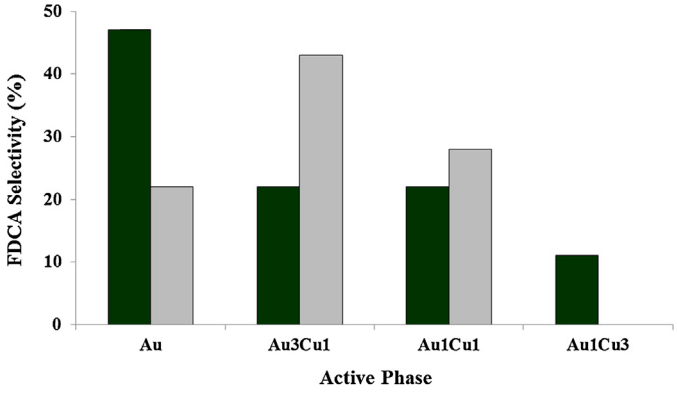

Fig. 6. Comparison of FDCA selectivity on CeO_2- and TiO_2-supported catalysts at different Au:Cu atomic ratios. Results are given at total conversion of HMF. The only products observed were FDCA and HMFCA. Reaction conditions: temperature 70 °C, reaction time 240 min, O_2 pressure 10 bar, HMF:metal:NaOH molar ratio 1:0.01:4. Legend: CeO_2, TiO_2.

in coil conformations; at low pH values, however, these aggregates become insoluble in water and tend to precipitate, due to their rearrangement.

Scientific literature extensively reports the positive effects of the addition of homogeneous bases on the performance of HMF oxidation. In reality, the rate of HMF oxidation depends significantly on the presence of NaOH, and the base seems to promote the formation of 5-hydroxymethyl-2-furancarboxylic acid (HMFCA), which can be further oxidized by the metal catalyst [18]. However, in the absence of an active catalyst, the basic environment leads to the formation of by-products that cannot be easily identified. Therefore, it is important to develop active catalysts that rapidly oxidize HMF and intermediate products, thus avoiding their fast degradation in reaction conditions.

3.2.2. *As-prepared samples: effect of the active phase composition*

It has been reported that the oxidation of HMF to FDCA over Au-based catalysts comprises two steps: (i) the aldehyde oxidation to HMFCA, and (ii) the oxidation of alcohol to FDCA, through the formation of 5-formyl-2-furancarboxylic acid (FFCA) as the reaction intermediate (Scheme 2) [16,20,21,49].

According to previous works, the formation of HMFCA via the hemiacetal [22] is a very fast reaction and is strongly influenced by the amount of base and reaction temperature, while the subsequent transformation of the hydroxyl group is slower [49]. Furthermore, the formation of 2,5-diformylfuran (DFF) has sometimes been observed, mainly in the absence of a base and with metals other than Au [15].

Firstly, the effect of Au:Cu ratio on the reactivity of CeO_2-supported catalysts was studied, for a total metal loading of 1.5 wt% (Fig. 5). Results indicate that pure ceria support is inactive in the oxidation, while forming very small amounts of HMFCA and by-products derived from HMF degradation. Conversely, the oxidation of HMF over Au and Au–Cu samples resulted in the formation of both HMFCA and FDCA. FFCA was observed only in low reaction time tests, whereas DFF was never formed.

For all samples, after 4 h reaction time HMF conversion was always complete, but considerable differences were seen among catalysts in terms of product selectivity. In particular, the selectivity toward FDCA decreased significantly for Cu-containing samples as compared to monometallic catalysts, due to the slower oxidation of HMFCA. TOF data – calculated as number of FDCA moles formed per unit time and per Au moles – turned out to be equal to 12.9 h^{-1}, 7.4 h^{-1} and 11.4 h^{-1} for Au–Ce, Au_3Cu_1–Ce, and Au_1Cu_1–Ce, respectively.

These results are very different from those observed with titania-supported materials [23], where the presence of Cu in the active phase led to a considerable improvement in catalytic performance as compared to Au-based materials. In particular, the comparison of the effect of Cu content using TiO_2 and CeO_2 supports (Fig. 6) indicates that the monometallic Au–Ce sample was the most active ceria-supported catalyst, while for titania-supported materials higher activity was observed with bimetallic systems. Indeed, the use of a CeO_2 support seems to depress the positive effect of Cu, instead observed in the case of titania-supported catalysts.

To discuss the reasons for the different behavior shown by CeO_2 and TiO_2, it must be reported that Au supported on ceria is very active in the oxidation of a variety of molecules [50,51]. In general, CeO_2 is known as an excellent redox support owing to its superior physicochemical properties as compared to conventional supports, due to the high number of oxygen vacancies and the easy Ce^{4+}/Ce^{3+} redox transition, with both significant oxygen mobility and storage capacity. Corma and co-workers showed that Au/CeO_2, especially in catalysts with nanocrystalline CeO_2 support, is particularly effective for the oxidation of alcohols to the corresponding aldehyde [52]. These catalysts were shown to be more active than the supported Pd catalysts available at that time [53]. Corma and Iborra [49] later showed that a similar catalyst was effective for the oxidation of HMF but reusable only to a limited extent.

The role of the CeO_2 support in gas phase reactions was reported to be correlated to its capacity either to facilitate oxygen transfer to the metal in order to stabilize cationic Au, or to activate molecular oxygen [54]. Moreover, several works [55–59] have demonstrated that all these events, i.e., oxygen mobility, activation of O_2, and cationic Au formation system are strongly dependent on Au–CeO_2 interfacial interaction.

In this work, the synthesis of Cu-containing nanoparticles required a considerable quantity of capping agent to control the growth of particles during preparation; this led to significantly larger amounts of organics around Cu-containing nanoparticles, which may prevent the proper interaction between the active phase and CeO_2, thus influencing the reactivity. As a matter of fact, the comparison of TPO profiles for monometallic and bimetallic samples (Fig. 7) indicates that the latter catalyst contains a significantly higher quantity of organics than the monometallic one. This is also confirmed by TG analysis, with the main combustion step shown at 230–240 °C, while the first small peak at 150 °C is ascribable to the desorption of CO_2 from the sample. This last signal is also present in the analysis of the CeO_2 support alone.

Due to the above-mentioned phenomena, and because a proper interaction between the active phase and the support appears to

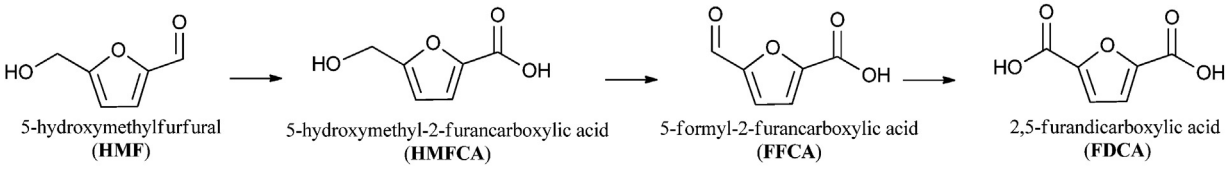

Scheme 2. The reaction scheme in HMF oxidation to FDCA.

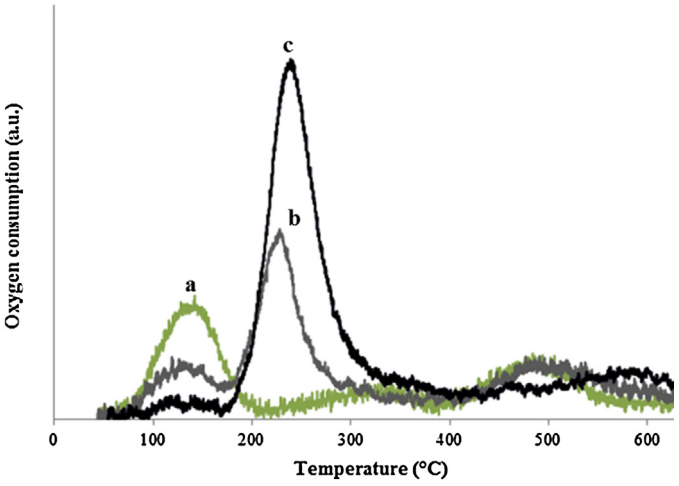

Fig. 7. TPO analysis of CeO_2 (a), Au–Ce (b) and Au_3Cu_1–Ce (c) catalysts.

be necessary in order to maximize the efficiency of these catalysts, we concluded that the greater amount of capping agent in Au–Cu bimetallic systems might be detrimental for the catalytic activity, being responsible in the end for the significant differences seen between TiO_2- and CeO_2-based systems. Indeed, the nanoparticle size effect on the activity could be ruled out because the size of the preformed nanoparticles was very similar for all catalysts regardless of the type of support, as demonstrated by XRD and TEM analysis.

In conclusion, the activity of TiO_2-supported catalysts seems to be more influenced by the nature of the nanoparticle species. Conversely, the activity of CeO_2-supported systems is mainly influenced by the interaction between Au and ceria; in this case, bimetallic nanoparticles were less active.

3.2.3. As-prepared samples: effect of reaction temperature and time

Catalytic experiments were also performed with the Au_3Cu_1–Ce catalyst by varying the reaction temperature (Fig. 8), while the activity was compared with the performance shown with the TiO_2 supported system containing the same active phase. A strong effect of temperature was observed on product distribution. The results obtained confirmed that the studied catalysts display a very high activity for the oxidation of the aldehydic functionality of HMF, forming a high quantity of HMFCA at low temperature also. Nevertheless, the oxidation of the primary alcohol side chain, which is necessary to form FDCA via intermediate FFCA, is more demanding and proceeds at a significant rate at temperatures higher than 80 °C. In both catalysts, after a 4-h reaction at 95 °C, a selectivity of FDCA higher than 90% was achieved. By-products were not detected under the reported conditions, and HMF was exclusively oxidized to HMFCA and then to FDCA.

A typical profile of products is shown in Fig. 9, where HMF conversion and products selectivity are plotted in function of reaction time with the Au–Ce catalyst at 95 °C. In these conditions, the complete conversion of HMF was obtained as soon as the reaction mixture reached the temperature of 95 °C. Since neither HMFCA nor 2,5-dihydroxymethylfurfural was formed in the absence of catalyst, the presence of the Cannizzaro reaction may be ruled out [60]. A very low amount of FFCA was seen during the initial stage of the reaction, but it rapidly converted into FDCA. Other by-products (e.g., DFF) were not formed, and after 4-h reaction time a very pure FDCA solution was obtained (Figure S2).

3.2.4. Catalyst stability and reusability

Since catalysts based on supported Au were reported to lose activity quickly, due to Au leaching and/or active phase blocking by competitive adsorption, the stability of the Au/CeO_2 and $Au–Cu/CeO_2$ catalysts was carefully studied. Figs. 10 and 11 show the results of the reusability studies using Au–Ce (Fig. 10) and Au_3Cu_1–Ce (Fig. 11). Unexpectedly, both monometallic and bimetallic catalysts showed a rapid increase in activity after

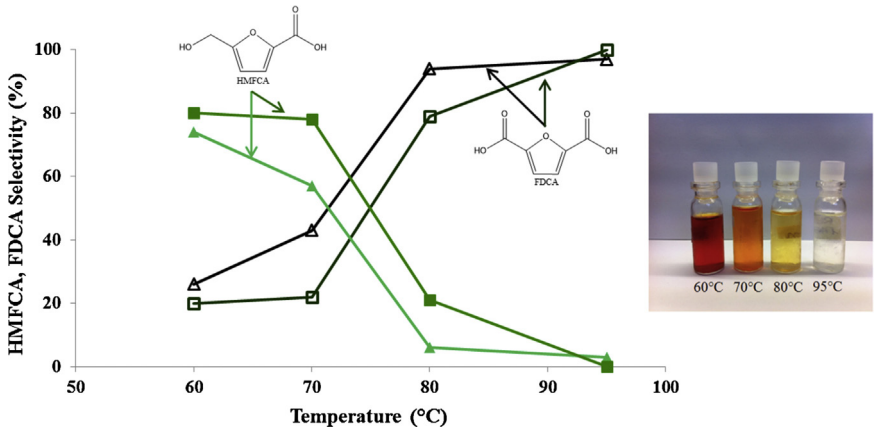

Fig. 8. HMFCA (closed symbols) and FDCA (open symbols) selectivity plotted in function of the reaction temperature with Au_3Cu_1–Ce (■, □) and Au_3Cu_1–Ti (▲, △) catalysts. For all reactions, the HMF conversion was total. The only products observed were FDCA and HMFCA. Reaction conditions: reaction time, 240 min, O_2 pressure 10 bar, HMF:metal:NaOH molar ratio 1:0.01:4. The inset shows the final mixture after reaction at different temperatures with Au_3Cu_1–Ti.

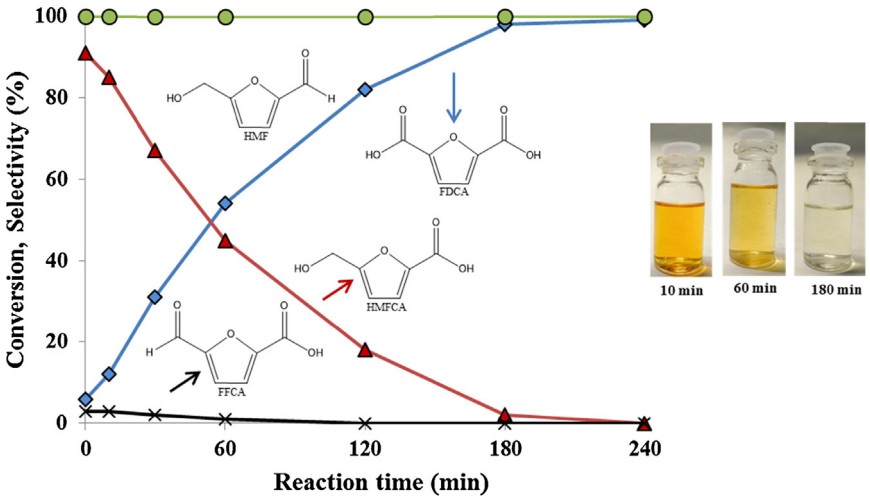

Fig. 9. HMF conversion and products selectivity plotted in function of reaction time with Au–Ce catalyst. Reaction conditions: temperature 95 °C, O_2 pressure 10 bar, HMF:metal:NaOH molar ratio 1:0.01:4. Legend: HMF conversion (●), HMFCA selectivity (▲), FFCA selectivity (×), FDCA selectivity (♦). Initial time (time zero) for the reaction is when the temperature of 95 °C was reached (after 15 min heating from a.t.). The inset shows the final mixture after reaction at different times.

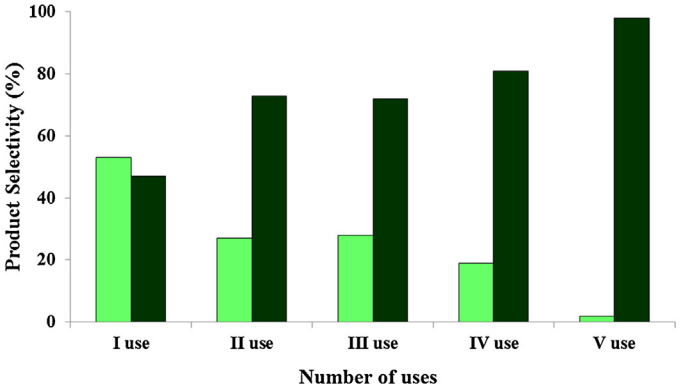

Fig. 10. Reusability study for the oxidation of HMF using Au–Ce catalyst. HMFCA (■) and FDCA (■) selectivities are given at total conversion. Reaction conditions: temperature 70 °C, reaction time 240 min, O_2 pressure 10 bar, HMF:metal:NaOH molar ratio 1:0.01:4.

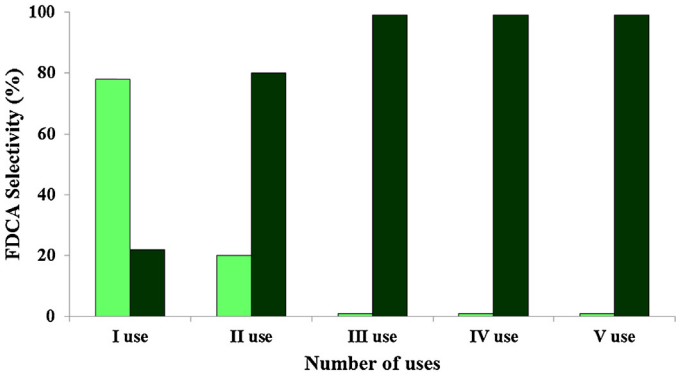

Fig. 11. Reusability study for the oxidation of HMF using Au_3Cu_1–Ce catalyst. HMFCA (■) and FDCA (■) selectivities are given at total conversion. Reaction conditions: temperature 70 °C, reaction time 240 min, O_2 pressure 10 bar, HMF:metal:NaOH molar ratio 1:0.01:4.

repeated catalytic tests. Similar trends were not observed in the case of TiO_2-supported materials [23,31]. In fact, in our previous papers we reported that with monometallic TiO_2-supported catalysts a rapid decline in activity was seen, while bimetallic Au–Cu materials were highly stable and resistant to poisoning. Since metal leaching during HMF oxidation was excluded by chemical analysis (XRF analysis revealed that no Au, Cu, or Ce species were dissolved in the reaction mixture), the unusual activation effect seen may be attributable to a modification of the interaction between the surface of the nanoparticles and CeO_2 during the reactivity experiments.

As already discussed, it is known that the changes brought about either by the support on metal particles or vice versa are mainly restricted to the atoms either at the interface or at the perimeter of the nanoparticles, where reactants can interact simultaneously with both the oxidic support and the metal catalyst. Moreover, reducible supports, such as CeO_2, can provide activated oxygen [61] and stabilize cationic gold [62]. These functions have been ruled out in Au-based catalysts when the latter are used in gas-phase reactions [63]. However, the capability of Au to activate CeO_2 is strongly improved by the interaction between the latter and metal particles, and this cooperative effect may be hindered by the presence of the residual capping agent (PVP) used.

On the other hand, it is likely that the removal of the capping agent takes place during reaction, thus increasing the support–nanoparticle interaction and leading to an increased activity during repeated uses. In order to verify this hypothesis, an in-depth study of the effect of the capping agent removal on Au and Au–Cu catalysts was performed.

3.2.5. *Treated catalysts: effect of capping agent removal*

Capping ligands such as surfactants and polymers are widely used for the synthesis of nanometals to control their size and shape [64]. Moreover, it has also been found that the ligands chemisorbed on the nanoparticles can hinder the reagents' access to the active surface [65–68]. PVP is among the most commonly used capping ligands in the chemical synthesis of nanometals. The wrapping of PVP around metal nanoparticles results in a metallic core-porous PVP shell architecture with a coordination of the carbonyl group and nitrogen atom of the pyrrolidone ring with the nanoparticle. Chemisorbed ligands were found to poison the catalytic activity of metals by lowering the accessibility of reactants to the metal surface [69]; moreover, it was observed that PVP interaction with metal nanocrystals is accompanied by charge transfer [70]. This interaction can modify the structure of metal colloids, sometimes with beneficial effects on the catalytic performance [71]. Indeed, Baumer's work reports a number of benefits that such ligand shells may have for heterogeneous catalysis, including the tuning of strong metal–support interaction (SMSI) effects [72].

Previous results obtained by our research group [23,31] demonstrated that the PVP presence over Au and Au–Cu TiO_2-supported catalysts does not prevent their activity in HMF oxidation. However, the catalysis over CeO_2-supported samples seems to indicate an important effect of the capping agent on both Au/CeO_2 and $Au–Cu/CeO_2$ catalysts; therefore, further experiments were conducted on these materials in order to investigate their catalytic behavior after removal of the PVP stabilizer.

Various studies have reported on the difficulties encountered during the removal of the residual capping agent from nanoparticles [73,74]. Various strategies, such as chemical and thermal treatments of catalysts [75,76] may be used. We tested two different treatments with the aim of obtaining surface-clean Au and Au–Cu species over CeO_2: (i) catalyst washing in autoclave using reaction conditions ($T = 70\,^{\circ}C$, 4 h, 10 bar of oxygen pressure, with metal:NaOH molar ratio equal to 0.01:4), but in the absence of HMF, and (ii) thermal treatment at $T = 300\,^{\circ}C$. The results obtained are summarized in Table 3.

The washing treatment of the Au–Ce sample in reaction conditions significantly boosted the activity; indeed, FDCA selectivity over this sample increased from 47% (Table 3, entry 1) to 92% (Table 3, entry 2). Gold-supported nanoparticles retained their dimension and TPO analysis confirmed that the catalyst surface was clean.

Similar results (FDCA selectivity 92%) were obtained by decomposing the capping agent through thermal treatment. TG and TPO analysis demonstrated the decomposition of PVP at this temperature. Nevertheless, the average size of Au nanoparticles, as evaluated by XRD and TEM on the calcined sample, underwent a slight increase, from 6 to 7.2 nm. This is not surprising, since Au nanoparticles are frequently seen to sinter after the thermal treatment carried out to remove organic ligands [66]; however, the low exothermicity associated with this treatment, due to the relatively low PVP content, made it possible to limit the particle growth.

The reported results indicate that the trend observed during repeated Au–Ce sample use is related to the PVP removal during reaction, and that the metal–CeO_2 interface plays a pivotal role in the oxidation of HMF.

The same treatments were carried out with the bimetallic catalyst Au_3Cu_1–Ce. The results obtained (Table 3, entries 4 and 5) indicate that the simple washing of the catalyst did not improve the catalytic activity at all, while the FDCA selectivity remained 22% after this treatment. As previously reported, it must be pointed out that Cu-containing nanoparticles were prepared with a higher PVP amount, due to the difficulty in controlling the particle growth in preformed Au–Cu sols; therefore, this high PVP content seems to be more difficult to remove. Moreover, the affinity of PVP with Au–Cu nanoparticles might be higher, due to the ability of PVP to form complex compounds with Cu [77].

Zhang and co-workers recently studied the removal of PVP on Au nanoparticles using $NaBH_4$ in water [78]; they demonstrated that the hydride derived from sodium borohydride has a higher binding affinity to nanoparticles than PVP. Moreover, a redox cycle was shown to remove PVP from nanoparticles [45]. These results might explain the different activation obtained by treating Au–Cu samples in reaction conditions either with HMF (during re-use tests) or without HMF (Table 3, entry 5); in fact, HMF oxidation may foster the displacement of PVP from the nanoparticle surface, thus inducing a higher metal–CeO_2 interaction while significantly increasing FDCA formation.

TPO analysis on Au_3Cu_1–Ce samples after pre-treatment in reaction conditions (Fig. 12) confirmed the incomplete removal of PVP from the catalyst surface. Although the TPO signal is significantly lower than that of the Au_3Cu_1–Ce sample before treatment – thus indicating that the washing procedure is effective in removing most of the PVP – the treatment might not completely eliminate the PVP

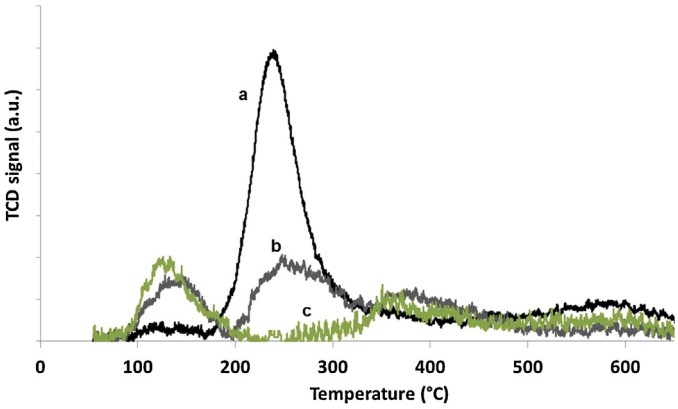

Fig. 12. TPO analysis of Au_3Cu_1–Ce catalysts. Legend: (a) untreated Au_3Cu_1–Ce; (b) Au_3Cu_1–Ce washed in reaction conditions; (b) Au_3Cu_1–Ce washed in reaction conditions and then calcined at 300 °C.

located at the interface between Au and CeO_2, with residual PVP still limiting the metal–support interaction.

Very different results were obtained after the thermal treatment of the Au_3Cu_1–Ce catalyst at 300 °C in air. In this case, the thermal treatment completely decomposed the stabilizer, which resulted in a significantly increased FDCA selectivity, from 22% (Table 3, entry 4) to 41% (Table 3, entry 6). However, the very high exothermicity entailed with PVP combustion strongly conditioned the average size of Au–Cu nanoparticles, which showed a considerable sintering phenomenon. In this case, the heat developed during the thermal treatment was higher than that for Au catalysts, because a higher PVP content was used to synthesize Au–Cu nanoparticles. Indeed, the particle size increased from 5 to 21 nm, thus making it difficult to discriminate–in the observed FDCA yield increase–among various effects, i.e. the influence of particle size, phase segregation, and metal-oxide interface. As a matter of fact, the activity in alcohol oxidation was reported to be affected by particle size; the optimum value was shown to be around 3–5 nm [79–81].

Nevertheless, our data demonstrate that large Au particles (size > 20 nm) are also able to oxidize HMF with high selectivity, if a suitable interaction with the ceria support is guaranteed. These data confirm some recently reported results on the conversion of aromatic alcohols [82] over unsupported bulk Au; those results showed that the interaction between the Au surface and the aromatic ring enhances the overall efficiency of the active site even in the presence of large particles.

In order to distinguish between the effect of particle size and that derived from PVP removal, the decomposition of PVP was also obtained by calcination of the Au_3Cu_1-Ce sample at 300 °C after washing in reaction conditions. The lower exothermicity, due to the lower stabilizer content, made it possible to control the particle size growth, which increased just to 11 nm, instead of the 21 nm for the unwashed sample. This two-stage decomposition of PVP significantly boosted the catalyst activity, while the FDCA selectivity increased from 41% (Table 3, entry 6) to 71% (Table 3, entry 7), thus confirming the significant effect of the active phase particle size on catalytic performance.

The mechanism of HMF reaction is still a matter of debate. Davis and co-workers [83] demonstrated the important role of hydroxyls for the liquid phase oxidation of alcohols to acids catalyzed by Au; they suggested that the role of O_2 in aqueous media is an indirect one, which does not involve direct incorporation into the acid, but rather regenerates hydroxide ions, by removing the electrons from the Au surface [84]. However, no comments are reported in literature regarding the possible role of CeO_2. Our results indicate that the metal–CeO_2 interface plays a pivotal role, similarly to what is observed in gas-phase reactions. Since the rate-controlling step

Table 3
Comparison of the selectivity to the reaction products obtained with treated and untreated catalysts (see text for details on the treatment procedure used). For all reactions the HMF conversion was total. Reaction conditions: temperature = 70 °C, reaction time 240 min, O_2 pressure 10 bar, HMF:metal:NaOH molar ratio 1:0.01:4.

Entry	Sample	Treatment	FDCA sel. (%)	HMFCA sel. (%)	Active phase dimension (nm)
1	Au–Ce	As is (dried 120 °C)	47	53	6.0
2	Au–Ce	Washed in reaction conditions	92	8	6.5
3	Au–Ce	Thermal treated 300 °C	91	9	7.2
4	Au_3Cu_1–Ce	As is (dried 120 °C)	22	78	5.0
5	Au_3Cu_1–Ce	Washed in reaction conditions	22	78	6.0
6	Au_3Cu_1–Ce	Thermal treated 300 °C	41	59	21.0
7	Au_3Cu_1–Ce	Washed in reaction conditions and thermal treated 300 °C	71	29	11.0

of the reaction appears to be the oxidation of HMFCA [53], it may be suggested that ceria acts as an oxygen (or hydroxyl) pump, by releasing and adsorbing the oxidizing species through the Ce^{+4}/Ce^{+3} redox process, as also suggested by Corma and co-workers [85]. Nevertheless, this effect is observed only in the presence of a close contact between metal and support, thus suggesting an important role of ceria defects induced by the metal presence [86].

4. Conclusions

The use of preformed metal nanoparticles with well-defined size and composition supported over titania or ceria was used to explore the role of the metal–support interaction in the oxidation of HMF over Au and Au–Cu catalysts. The deposition of preformed nanoparticles is not support-dependent [87], a fact that made it possible to investigate the support effect on the activity and selectivity in HMF oxidation to FDCA. The results obtained demonstrate that CeO_2 is the most effective support for obtaining active and selective catalysts for FDCA synthesis. Check unsited referenceuniform nanoparticles, used for catalyst preparation, were surface-bound by poly(N-vinyl-2-pyrrolidone) (PVP), the organic capping agents used for nanoparticle synthesis, and the presence of this stabilizer hindered the chemical interaction between the active phase and CeO_2. Indeed, pre-treatment of catalysts was necessary in order to remove the PVP, enable the interaction between ceria and metal nanoparticles at the interface, and ultimately activate the catalyst, events which led to the enhancement of the catalytic performance.

Acknowledgements

The University of Bologna is acknowledged for financial support through the FARB Project “Catalytic transformation of biomass-derived materials into high added-value chemicals”, 2014–2015. INSTM is acknowledged for co-financing the PhD project of A.L.

Appendix A. Supplementary data

Supplementary material related to this article can be found, in the online version, at http://dx.doi.org/10.1016/j.apcatb.2014.08.026.

References

[1] J.N. Chheda, G.W. Huber, J.A. Dumesic, Angew. Chem. Int. Ed. 46 (2007) 7164–7183.
[2] R.A. Sheldon, Green Chem. 16 (2014) 950–963.
[3] M. Vohra, J. Manwar, R. Manmode, S. Padgilwar, S. Patil, J. Environ. Chem. Eng. 2 (2014) 573–584.
[4] L. Luque, R. Westerhof, G. van Rossum, S. Oudenhoven, S. Kersten, F. Berruti, L. Rehmann, Bioresour. Technol. 161 (2014) 20–28.
[5] S. Dutta, S. De, B. Saha, Biomass Bioenerg. 55 (2013) 355–369.
[6] A. Corma, S. Iborra, A. Velty, Chem. Rev. 107 (2007) 2411–2502.
[7] M.J. Climent, A. Corma, S. Iborra, Green Chem. 16 (2014) 516–547.
[8] J.N. Chheda, Y. Roman-Leshkov, J.A. Dumesic, Green Chem. 9 (2007) 342–350.
[9] T. Werpy, G. Petersen, Top Value Added Chemicals From Biomass, 2004 http://www1.eere.energy.gov/bioenergy/pdfs/35523.pdf
[10] F. Yang, Q. Liu, X. Bai, Y. Du, Bioresour. Technol. 102 (2011) 3424–3429.
[11] R.J. van Putten, J.C. van der Waal, D. de Jong, C.B. Rasrendra, H.J. Heeres, J.G. de Vries, Chem. Rev. 113 (2013) 1499–1597.
[12] F. Koopman, N. Wierckx, J.H. de Winde, H.J. Ruijssenaars, Bioresour. Technol. 101 (2010) 6291–6296.
[13] W.P. Dijkman, D.E. Groothuis, M.W. Fraaije, Angew. Chem. Int. Ed. 53 (2014) 6515–6518.
[14] C. Munoz de Diego, P.W. Shammel, M.A. Dam, G.J.M. Gruter, WO Patent 2011/043660 (2011), assigned to Furanix Technologies BV.
[15] M.A. Lilga, R.T. Hallen, J. Hu, J.F. White, M.J. Gray, US 2010/0152470 (2010), assigned to Battelle Memorial Institute.
[16] A. Shalkh, D.R. Parker, M.E. Janka, L.R. Partin, US Patent 2014/0142328 (2014), assigned to Eastman Chemical Company.
[17] Y.Y. Gorbanev, S.K. Klitgaard, J.M. Woodley, C.H. Christensen, A. Riisager, ChemSusChem 2 (2009) 672–675.
[18] S.E. Davis, B.N. Zope, R.J. Davis, Green Chem. 14 (2012) 143–147.
[19] A.A. Rosatella, S.P. Simeonov, R.F.M. Frade, C.A.M. Afonso, Green Chem. 13 (2011) 754–793.
[20] C. Moreau, M.N. Belgacem, A. Gandini, Top. Catal. 27 (2004) 11–30.
[21] J. Cai, H. Ma, J. Zhang, Q. Song, Z. Du, Y. Huang, J. Xu, Chem. Eur. J. 19 (2013) 14215–14223.
[22] N.K. Gupta, S. Nishimura, A. Takagaki, K. Ebitani, Green Chem. 13 (2011) 824–827.
[23] T. Pasini, M. Piccinini, M. Blosi, R. Bonelli, S. Albonetti, N. Dimitratos, J.A. Lopez-Sanchez, M. Sankar, Q. He, C.J. Kiely, G.J. Hutchings, F. Cavani, Green Chem. 13 (2011) 2091–2099.
[24] A. Villa, M. Schiavoni, S. Campisi, G.M. Veith, L. Prati, ChemSusChem 6 (2013) 609–612.
[25] N. Semagina, L. Kiwi-Minsker, Catal. Rev. Sci. Eng. 51 (2009) 147–217.
[26] N. Yan, Y. Yuan, P.J. Dyson, Chem. Commun. 47 (2011) 2529–2531.
[27] H. Ziaei-azad, C.-X. Yin, J. Shen, Y. Hu, D. Karpuzov, N. Semagina, J. Catal. 300 (2013) 113–124.
[28] N. Toshima, Y. Wang, Langmuir 10 (1994) 4574–4580.
[29] L.M. Rossi, L.L.R. Vono, M.A.S. Garcia, T.L.T. Faria, J.A. Lopez-Sanchez, Top. Catal. 56 (2013) 1228–1238.
[30] N. Dimitratos, J.A. Lopez-Sanchez, G.J. Hutchings, Chem. Sci. 3 (2012) 20–44.
[31] S. Albonetti, T. Pasini, A. Lolli, M. Blosi, M. Piccinini, N. Dimitratos, J.A. Lopez-Sanchez, D.J. Morgan, A.F. Carley, G.J. Hutchings, F. Cavani, Catal. Today 195 (2012) 120–126.
[32] M. Blosi, S. Albonetti, M. Dondi, G. Baldi, A. Barzanti, PCT/EP2010/052534 (2010), assigned to Colorobbia.
[33] J. Yin, S. Shan, L. Yang, D. Mott, O. Malis, V. Petkov, F. Cai, M. Shan Ng, J. Luo, B.H. Chen, M. Engelhard, C.J. Zhong, Chem. Mater. 24 (2012) 4662–4674.
[34] J.C. Bauer, D. Mullins, M. Li, Z. Wu, E.A. Pyzant, S.H. Overbury, S. Dai, Phys. Chem. Chem. Phys. 13 (2011) 2571–2581.
[35] C.L. Bracey, P.R. Ellis, G.J. Hutchings, Chem. Soc. Rev. 38 (2009) 2231–2243.
[36] J.C. Bauer, G.M. Veith, L.F. Allerd, Y. Oyola, S.H. Overbury, S. Dai, ACS Catal. 2 (2012) 2537–2546.
[37] X. Liu, A. Wang, L. Li, T. Zhang, C.Y. Mou, J.F. Lee, J. Catal. 278 (2011) 288–296.
[38] K. An, S. Alayoglu, T. Ewers, G.A. Somorjai, Colloid Interface Sci. J. 373 (2012) 1–13.
[39] I. Miguel-García, Á. Berenguer-Murcia, D. Cazorla-Amorós, Appl. Catal. B 98 (2010) 161–170.
[40] M. Blosi, S. Albonetti, G. Baldi, F. Gatti, M. Dondi, Dyes Pigments 4 (2) (2012) 355–362.
[41] S. Albonetti, M. Blosi, F. Gatti, A. Migliori, L. Ortolani, V. Morandi, G. Baldi, M. Dondi, Stud. Surf. Sci. Catal. 175 (2010) 621–624.
[42] M. Blosi, S. Albonetti, S. Ortelli, A.L. Costa, L. Ortolani, M. Dondi, New J. Chem. 38 (2014) 1401–1409.
[43] E. Bayrakdar, T. Gürkaynak Altınçekiç, M.A. Faruk Öksüzömer, Fuel Process. Technol. 110 (2013) 167–175.
[44] C. Kim, H. Lee, Catal. Commun. 10 (2009) 1305–1309.
[45] R.M. Rioux, H. Songa, M. Grass, S. Habas, K. Niesz, J.D. Hoefelmeyer, P. Yang, G.A. Somorjai, Top. Catal. 39 (2006) 167–174.
[46] K.R. Vuyyuru, P. Strasser, Catal. Today 195 (2012) 144–154.
[47] K.R.S. Patil, C.R.F. Lund, Energy Fuels 25 (2011) 4745–4755.
[48] A. Piccolo, P. Conte, A. Cozzolino, Eur. J. Soil Sci. 50 (1999) 687–694.
[49] O. Casanova, S. Iborra, A. Corma, ChemSusChem 2 (2009) 1138–1144.
[50] R. Si, M. Flytzani-Stephanopoulos, Angew. Chem. Int. Ed. 47 (2008) 2884–2887.

[51] J.L. He, T. Xu, Z.H. Wang, Q.H. Zhang, W.P. Deng, Y. Wang, Angew. Chem. Int. Ed. 51 (2012) 2438–2442.
[52] A. Abad, P. Concepción, A. Corma, H. García, Angew. Chem. Int. Ed. 44 (2005) 4066–4069.
[53] K. Mori, T. Hara, T. Mizugaki, K. Ebitani, K. Kaneda, J. Am. Chem. Soc. 26 (2004) 10657–10666.
[54] M. Cargnello, P. Fornasiero, R.J. Gorte, Catal. Lett. 142 (2012) 1043–1048.
[55] P. Lakshmanan, F. Averseng, N. Bion, L. Delannoy, J.-M. Tatibouët, C. Louis, Gold Bull. 46 (2013) 233–242.
[56] V.V. Pushkarev, V.I. Kovalchuk, J.L. d'Itry, J. Phys. Chem. B 108 (2004) 5341–5348.
[57] C. Li, K. Domen, K. Maruya, T. Onishi, J. Catal. 123 (1990) 436–442.
[58] C. Oliva, G. Termignone, F.P. Vatti, L. Forni, A.V. Vishniakov, J. Mater. Sci. 31 (1996) 149–158.
[59] D. Martin, D. Duprez, J. Phys. Chem. 100 (1996) 9429–9438.
[60] S. Subbiah, S.P. Simeonov, J.M.S.S. Esperança, L. Paulo, N. Rebelo, C.A.M. Afonso, Green Chem. 15 (2013) 2849–2853.
[61] L. Kundakovic, M. Flytzani-Stephanopoulos, J. Catal. 179 (1998) 203–221.
[62] M. Wang, F. Wang, Ji. Ma, M. Li, Z. Zhang, Y. Wang, X. Zhang, J. Xu, Chem. Commun. 50 (2014) 292–294.
[63] M.J. Beier, T.W. Hansen, J.-D. Grunwaldt, J. Catal. 266 (2009) 320–330.
[64] Y.N. Xia, Y.J. Xiong, B. Lim, S.E. Skrabalak, Angew. Chem. Int. Ed. 48 (2009) 60–103.
[65] A. Villa, D. Wang, D.S. Su, L. Prati, ChemCatChem 1 (2009) 510–514.
[66] G.A. Somorjai, H. Frei, J.Y. Park, J. Am. Chem. Soc. 131 (2009) 16589–16605.
[67] H. Tsunoyama, N. Ichikuni, H. Sakurai, T. Tsukuda, J. Am. Chem. Soc. 131 (2009) 7086–7093.
[68] C. Evangelisti, N. Panziera, A. D'Alessio, L. Bertinetti, M. Botavina, G. Vitulli, New J. Catal. 272 (2010) 246–252.
[69] A. Quintanilla, V.C.L. Butselaar-Orthlieb, C. Kwakernaak, W.G. Sloof, M.T. Kreutser, F. Kapteijn, J. Catal. 271 (2010) 104–114.
[70] Y. Borodko, S.M. Humphrey, T.D. Tilley, H. Frei, G.A. Somorjai, J. Phys. Chem. C 111 (2007) 6288–6295.
[71] K. Chen, H. Wu, Q. Hua, S. Chang, W. Huang, Phys. Chem. Chem. Phys. 15 (2013) 2273–2277.
[72] P. Sonstrom, M. Baumer, Phys. Chem. Chem. Phys. 13 (2011) 19270–19284.
[73] S.O. Blavo, E. Qayyum, L.M. Baldyga, V.A. Castillo, M.D. Sanchez, K. Warrington, M.A. Barakat, J.N. Kuhn, Top. Catal. 56 (2013) 1835–1842.
[74] Z. Niu, Y. Li, Chem. Mater. 26 (2014) 72–83.
[75] L.R. Baker, G. Kennedy, J.M. Krier, M. Van Spronsen, R.M. Onorato, G.A. Somorjai, Catal. Lett. 142 (2012) 1286–1294.
[76] J.A. Lopez-Sanchez, N. Dimitratos, C. Hammond, G.L. Brett, L. Kesavan, S. White, P. Miedziak, R. Tiruvalam, R.L. Jenkins, A.F. Carley, D. Knight, C.J. Kiely, G.J. Hutchings, Nat. Chem. 3 (2011) 551–556.
[77] S. Fernandes, H.-S. Kim, R. Hatti-Kaul, Protein Express. Purif. 24 (2002) 460–469.
[78] S.M. Ansar, F.S. Ameer, W. Hu, S. Zou, C.U. Pittman, D. Zhang, Nano Lett. 13 (2013) 1226–1229.
[79] W.C. Ketchie, Y.-L. Fang, M.S. Wong, M. Murayama, R.J. Davis, J. Catal. 250 (2007) 94–101.
[80] F. Li, Q.H. Zhang, Y. Wang, Appl. Catal. A 334 (2008) 217–226.
[81] S.E.J. Hackett, R.M. Brydson, M.H. Gass, I. Harvey, A.D. Newman, K. Wilson, Angew. Chem. Int. Ed. 46 (2007) 8593–8596.
[82] H. Guo, A. Al-Hunaiti, M. Kemell, S. Rautiainen, M. Leskela, T. Repo, ChemCatChem 3 (2011) 1872–1875.
[83] M.S. Ide, R.J. Davis, Acc. Chem. Res. 47 (2014) 825–833.
[84] B.N. Zope, D.D. Hibbitts, M. Neurock, R.J. Davis, Science 330 (2010) 74–78.
[85] O. Casanova, S. Iborra, A. Corma, J. Catal. 265 (2009) 109–116.
[86] H.-F. Li, N. Zhang, P. Chen, M.-F. Luo, J.-Q. Lu, Appl. Catal. B 110 (2011) 279–285.
[87] N.F. Zheng, G.D. Stucky, J. Am. Chem. Soc. 128 (2006) 14278–14280.